Structural Transitions from Pyramidal to Fused Planar to Tubular to Core/Shell Compact in Gold Clusters: Au_n^- ($n = 21-25$)

Satya Bulusu,[†] Xi Li,[‡,§] Lai-Sheng Wang,[‡,*] and Xiao Cheng Zeng[†,*]

Department of Chemistry and Nebraska Center for Materials and Nanoscience, University of Nebraska—Lincoln, Lincoln, Nebraska 68588, Department of Physics, Washington State University, 2710 University Drive, Richland, Washington 99354, and Chemical Sciences Division, Pacific Northwest National Laboratory, MS K8-88, P.O. Box 999, Richland, Washington 99352

Received: December 23, 2006

We report a joint theoretical and experimental study of low-lying structures and structural transitions of gold cluster anions Au_n^- in the size range of $n = 21-25$. Well-resolved photoelectron spectra are used to compare with density functional theory calculations and to identify the low-lying structures of the gold cluster anions. Due to the high stability of the tetrahedral Au_{20}, the pyramid-based structures are found to be competitive for $n = 21-23$. In addition to the pyramid-based structures, global-minimum searches also reveal two other generic structural types of low-lying clusters in the size range of $n = 21-24$, namely, the fused-planar and the hollow-tubular structures. At $n = 24$, the pyramid-based structures are no longer competitive and the hollow-tubular structures dominate the low-lying population. At $n = 25$, a structural transition from hollow-tubular to core/shell compact structure is observed.

Introduction

Gold nanoclusters have attracted considerable attention due to their wide-ranging applications in catalysis, sensors, and bioconjugate probes.[1−6] Experimental and theoretical studies have revealed that gold clusters exhibit some unique properties such as strong relativistic effects.[5] The strong relativistic effect leads to reduced 5d−6s energy gap and strong s−d hybridization.[7] A possible consequence of the strong relativistic effect is that small gold cluster anions Au_n^- tend to form two-dimensional (2D) planar structures for $n \leq 13$,[7,8] a surprising finding that has been confirmed subsequently.[9−19] For medium-sized gold cluster anions, Au_{20}^- has been found to be a perfect tetrahedral pyramidal cluster.[20] A previous joint photoelectron spectroscopy (PES) and theoretical study showed that a structural transition from 2D to three-dimensional (3D) shell-like structures occurs at $n = 13$.[10] A recent PES and theoretical investigation found a remarkable transition to hollow-cage structures at $n = 16$, and a transition to pyramidal structure at $n = 18-19$.[21] These observations have been further substantiated by more recent theoretical calculations[22] and an electron diffraction study.[23] For larger gold anion clusters such as Au_{55}^-, previous experimental and theoretical studies showed that they favor low-symmetry compact structures due to the strong relativistic effects.[24,25]

Increasing research efforts have been recently directed toward the exploration of structural evolution of gold clusters in the size range of $20 < n < 55$. It is worthy to note that, besides the low-symmetry compact structures, previous theoretical studies have also suggested the possible existence of highly symmetric hollow-cage structures Au_{32}, Au_{42}, and Au_{50},[26−31] as well as hollow-tubular structure Au_{26}.[32] However, a recent joint experimental PES and theoretical study indicated that the anion Au_{32}^- is not a hollow cage, but most likely exhibits a core/shell compact structure.[33] This conclusion suggests that the core/shell compact structures which contain interior (endohedral) atoms are more populated in the cluster beam than the less compact hollow-cage structures for clusters as large as Au_{32}^-. One major goal of the current study is to identify the size range of clusters in which the transition from the pyramidal to core/shell compact structure occurs.

Experimental and Theoretical Methods

Photoelectron Spectroscopy. The PES experiment was done similarly as for the smaller-sized gold clusters.[10,20,21] The gold anion clusters were produced using a laser vaporization of a pure gold disk target and mass analyzed using time-of-flight mass spectrometry.[34] The clusters of interest in the size range of Au_n^- for $n = 21-25$ were each selected and decelerated before being detached by a laser beam. PES spectra were obtained using a magnetic-bottle time-of-flight photoelectron analyzer, which features a 3.5 m long electron flight tube. For the current study, PES spectra (Figures 1−6) were measured at two photon energies, 266 nm (4.661 eV) and 193 nm (6.424 eV), calibrated with the known spectrum of Au^-. The electron energy resolution was $\Delta E/E \sim 2.5\%$, i.e., 25 meV for 1 eV electrons.

Theoretical Methods. The computational search for the lowest-energy structures was performed using the basin-hopping method[35] for gold anion clusters Au_n^- in the size range $n = 21-25$. We combined the global-minimum search method directly with density functional theory (DFT) calculations using effective core potentials.[21,22] Both unbiased and motif-based constrained searches[36] were performed. During the search, a geometry minimization was carried out after each accepted Monte Carlo move. DFT calculations using the generalized-gradient approximation (GGA) with the Perdew−Burke−Ernzerhof (PBE) exchange-correlation functional[37] and the

[†] University of Nebraska—Lincoln.
[‡] Washington State University and Pacific Northwest National Laboratory.
[§] Current address: Rowland Institute at Harvard, Harvard University, 100 Edwin H. Land Blvd., Cambridge, MA 02142.
* E-mails: xczeng@phase2.unl.edu (X.C.Z.); ls.wang@pnl.gov (L.S.W.).

10.1021/jp068897v CCC: $37.00
Published on Web 02/27/2007

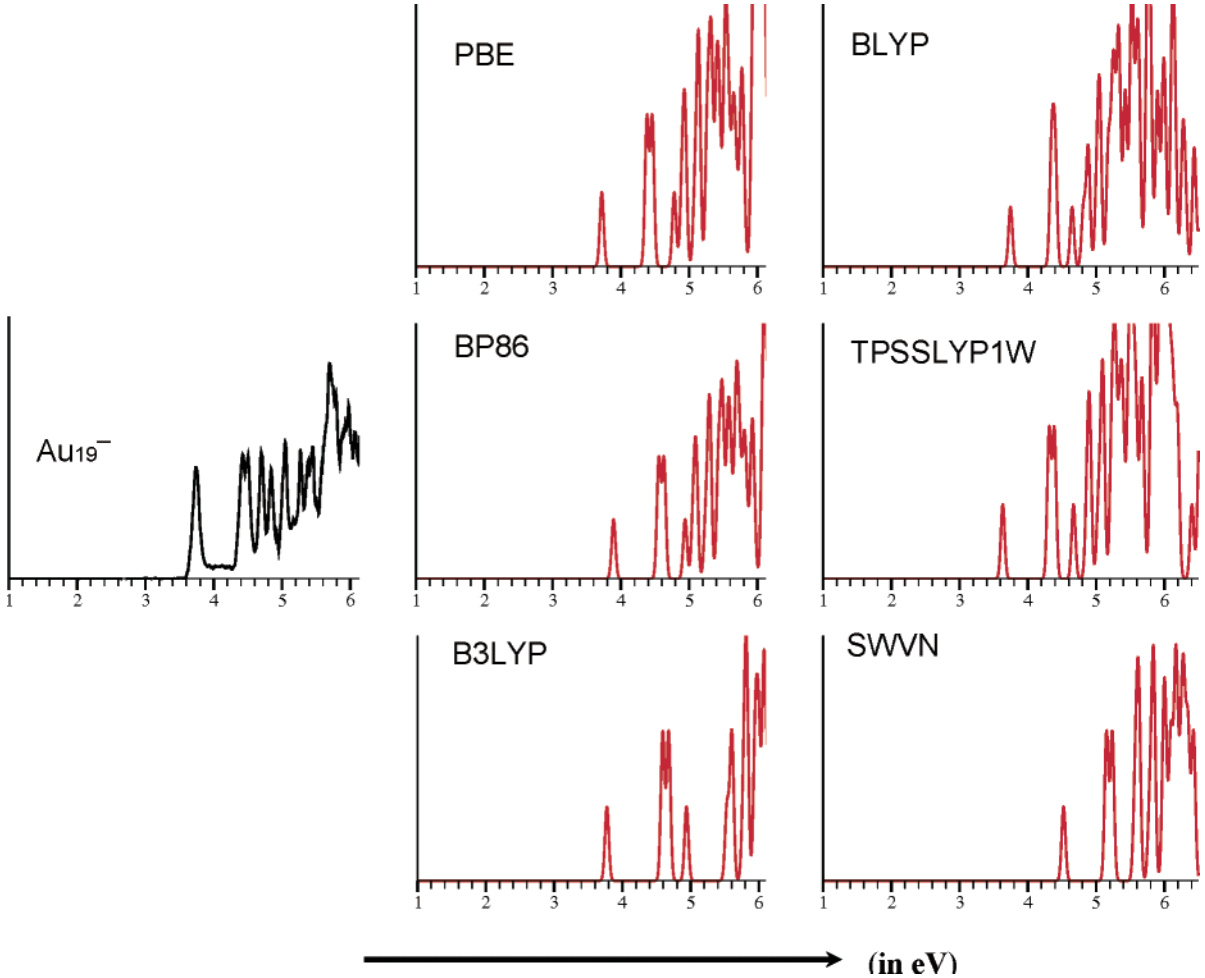

Figure 1. Comparison of the 193 nm photoelectron spectrum (black line) to the simulated PES spectra (red lines) for the lowest-energy pyramidal isomer of Au_{19}^-. The simulated PES spectra were calculated using six different density functionals, including three GGA functionals (PBE, BLYP, and BP86), one metal-GGA functional (TPSSLYP1W), one hybrid functional (B3LYP), and one LDA functional (SWVN), all with the LANL2DZ basis set. The x-axis represents binding energy (in eV).

double numerical polarized (DNP) basis set implemented in the DMol[3] code[38] were used for the geometric optimization. Those low-lying isomers whose PBE/DNP energy value within 0.3 eV from the lowest-lying isomer are all regarded as candidates for the lowest-energy structure due to error bars of a few tenths of an electronvolt for DFT total-energy calculations (see Table 1).[15,16,22] For the candidate low-lying isomers, their geometries were reoptimized (Figures 2−6) using the PBE functional and the scalar relativistic LANL2DZ basis set, implemented in Gaussian 03 package.[39] Total energies of these isomers and relative energies with respect to the lowest-energy isomer (in the PBE calculation using PBEPBE/LANL2DZ key words[39]) are shown in Table 1 (Au_{21}^-) and Table 2 (Au_{22}^- to Au_{25}^-). In addition, we carried out single-point energy calculations for the top-five isomers of Au_{21}^- using the second-order Moller−Plesset perturbation (MP2) level of theory with the LANL2DZ basis set (Table 1).

Last, simulated anion photoelectron spectra[10,20,21,33] based on the DFT calculations with the PBE/LANL2DZ functional/basis set for a number of low-lying isomers are computed (red-colored lines in Figures 1−5). Note that the selection of PBE GGA functional is based on a benchmark test with six different functionals for the pyramidal gold anion Au_{19}^-, since this isomer is the sole candidate for the global minimum of Au_{19}^-.[21] The selected functionals include three GGA functionals (PBE, BLYP, and BP86),[40−42] one functional within the local-density approximation (LDA),[43] one meta-GGA functional in which the functional depends kinetic energy density also (here we used the TPSSLYP1W functional,[39] which denotes the exchange functional of Tao, Perdew, Staroverov, and Scuseria[44] and the correlation function of Lee, Yang, and Parr[41]), and one hybrid functional (B3LYP).[41,45] In Figure 1, we displayed the measured (black line) and simulated (red lines) PES spectra for Au_{19}^-. We found that the SWVN and BP86 functionals give inaccurate vertical detachment energy, B3LPY predicts larger energy gap between the first and second peaks, compared to the measured energy gap, and BLYP does not predict a doublet feature in the second peak. Both PBE and TPSSLYP1W functionals provide excellent overall match to the measured PES spectra although the PBE gives slightly better prediction for the location of the first and second peak than the TPSSLYP1W functional. Hence, the PBE functional was selected for calculating PES spectra shown in Figures 2−6.

Results and Discussions

The experimental PES data with numerous well-resolved peaks are shown in Figures 2−6 (black curves). The electron binding energies display a clear odd−even effect with the odd-sized cluster exhibiting higher electron binding energies than their even-sized neighbors. This observation suggests that all the odd-sized anions Au_n^- have closed shell electron configura-

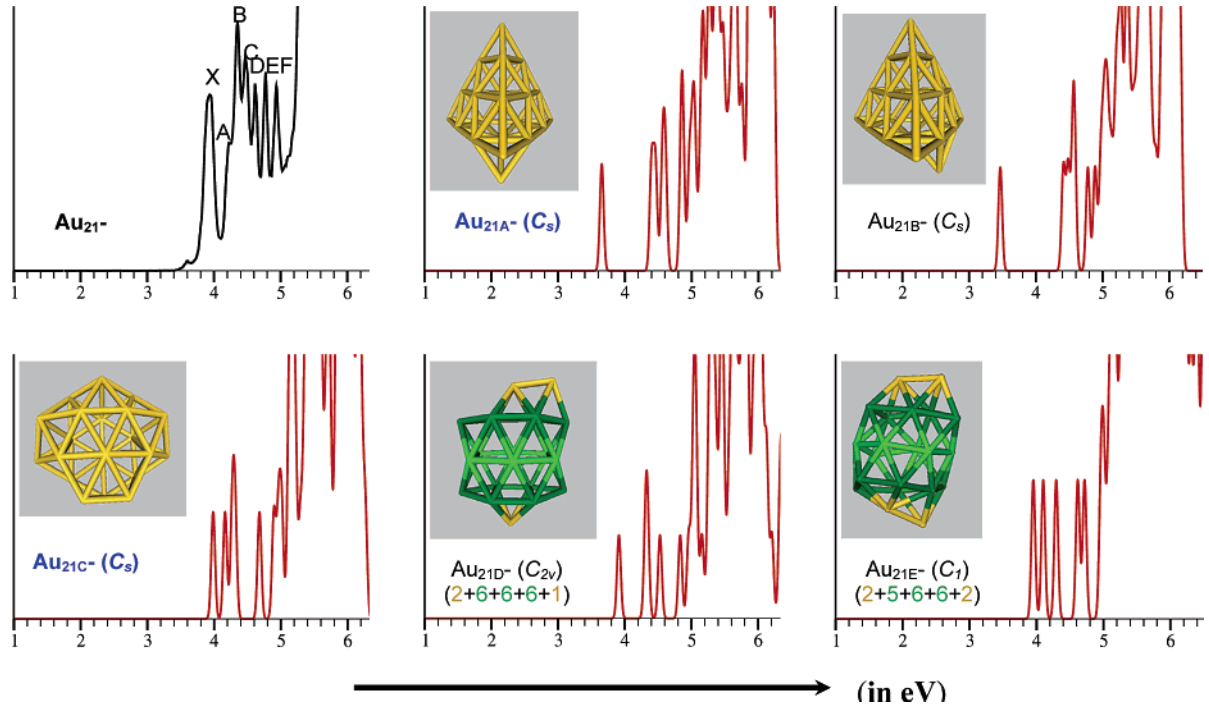

Figure 2. Photoelectron spectrum (black line) measured at 193 nm (6.424 eV) compared to the simulated PES spectra (red lines) of five low-lying isomers of cluster Au_{21}^- obtained from the unbiased global-minimum search. The *x*-axis represents binding energy (in eV). The tubular motif structures are highlighted by the green color. Notations 2+6+6+6+1 and 2+5+6+6+2 are introduced for the hollow-tubular structures, where the number denotes the number of gold atoms in each "layer". The two isomers whose index is highlighted by blue give the best overall fit to the measured spectra.

TABLE 1: Electronic Energies (in a.u.) of the Five Low-Lying Isomers of Cluster Au_{21}^- Calculated at PBEPBE/LANL2DZ and MP2/LANL2DZ//PBEPBE/LANL2DZ Levels of Theory, and the Relative Energies ΔE (in eV) with Respect to the Lowest-Energy Cluster[a]

Au_{21}^-	PBEPBE/LANL2DZ	ΔE	MP2/LANL2DZ//PBEPBE/LANL2DZ	ΔE
A	−2845.6197074	**0.000**	−2828.2837003	**1.153**
B	−2845.6145172	0.141	−2828.2822739	1.192
C	−2845.6078893	**0.322**	−2828.3260759	**0.000**
D	−2845.6040476	0.426	−2828.3061779	0.541
E	−2845.5995952	0.547	−2828.3097993	0.443

[a] Bold-faced values denote the primary and supplementary isomers whose simulated PES spectra match the measured spectrum.

tions, whereas the even-sized neutral Au_n are closed shell. HOMO−LUMO gaps are clearly shown in the PES spectra of $n = 22$ and 24. In particular, Au_{24}^- shows a relatively clean gap between the first and second features while the spectrum of Au_{22}^- suggests the existence of multiple isomers.

In the unbiased searches, typically about 200 structurally different low-energy isomers for each Au_n^- ($n = 21-25$) were generated. We thus obtained quite a large population of low-energy isomers. PES spectra of the leading candidates from both the unbiased and motif-based (constrained) searches were computed and compared with the experimental PES spectra to identify the best match and to examine any new generic structures (or motifs).

Because of the existence of multiple low-lying isomers, one can see from Figures 2 and 3 that, unlike the Au_{19}^- case (Figure 1), no single cluster for $n = 21-23$ can give an overall good match to the locations of the first few peaks (marked by letter X, A−F) within the 3.5−5 eV binding-energy range of the measured PES spectra. Depending on the degree of fit, however, one isomer can be classified as the *primary* isomer, which can yield the best match to the location of the first few major peaks. The experimental vertical detachment energies (VDEs), defined by the location of the first intense peak near the threshold, are given in Table 3, and are compared with the VDEs of the simulated spectra of the *primary* low-lying isomers. An additional *supplementary* isomer was identified respectively for $n = 21-23$ to match some *weaker* features between the first and second intense peaks. Most other isomers can be ruled out due to large discrepancy in patterns of PES spectra between the theory and experiment.

Au_{21}^-. For Au_{21}^-, the top-five low-lying isomers obtained from the unbiased global-minimum search are shown in Figure 2. Among the five, Au_{21A}^- and Au_{21B}^- are based on the highly stable pyramidal structure of Au_{20}^- with one additional atom bonded to either the corner or the edge, whereas Au_{21C}^- can be viewed as fusion of two planar gold structures at the edge, and Au_{21D}^- and Au_{21E}^- can be viewed as hollow-tubular structures, where the middle portion of the clusters is tube-like, consisting of stacked five- or six-membered rings. Thus, Au_{21D}^- and Au_{21E}^- can be also viewed as built upon a tube-like motif (highlighted by green color in Figure 2). Note that in Figure 2 we also introduced notations for the hollow-tubular structures Au_{21D}^- and Au_{21E}^-, namely 2+6+6+6+1 and 2+5+6+6+2, where the number denotes the number of gold atoms in each "layer".

As pointed out above, when we compared the simulated PES with the experimental PES spectra we focused mainly on the location of the first few peaks between 3 and 5 eV, particularly the VDE. The two pyramidal isomers Au_{21A}^- and Au_{21B}^- yield similar PES spectra, each with a peak at low VDE followed by a relatively large energy gap, reminiscent of the large HOMO−LUMO gap of the tetrahedral Au_{20} parent cluster.[20] The first peak of these two isomers agrees well with a weak signal around

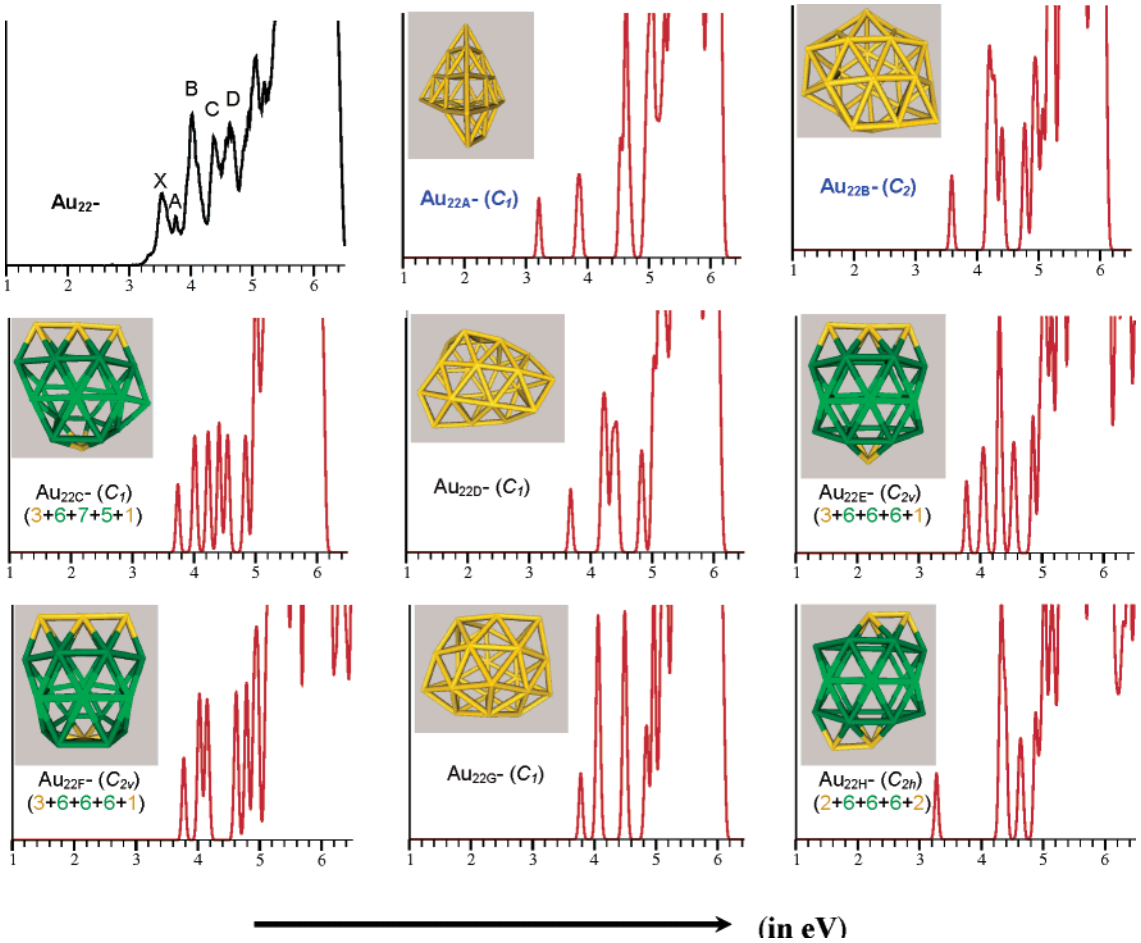

Figure 3. Photoelectron spectrum (black line) measured at 193 nm compared to the simulated PES spectra (red lines) of eight low-lying isomers of cluster Au_{22}^-. The *x*-axis represents binding energy (in eV). The two isomers whose index is highlighted by blue give the best overall fit to the measured spectra.

3.6 eV in the experimental data (Figure 2), suggesting that the pyramidal isomers were weakly populated in the cluster beam. Note also that although the DFT calculation suggests that Au_{21A}^- and Au_{21B}^- are the two lowest-energy isomers, the MP2 calculation indicates that these two isomers become appreciably higher in energy among the five low-lying isomers (Table 1). The MP2 results demonstrate again that for topologically very different gold isomers, the energy ranking obtained from DFT calculations is less reliable since the error bar in the relative-energy calculation can amount to a few tenths of an electron-volt.[15,16,22]

Among the remaining three isomers, the fused-planar isomer Au_{21C}^- which is the lowest-energy isomer at the MP2 level is a good candidate for the *primary* isomer since the first three peaks of Au_{21C}^- match the X, A, and B features of the measured spectrum (Figure 2) fairly well, and, to some extent, match the intense peaks D and F. The primary isomer Au_{21C}^- and a supplementary isomer Au_{21A}^- provide reasonable fit to the first seven features (X, A−F) of the measured spectrum. Both isomers are likely to coexist in the cluster beam.

Recently, Xing et al.[23] also reported low-lying hollow-tubular structures of Au_{21}^-. In particular, Xing et al. found that a 3+6+6+4+2 isomer (21IV in ref 23) gives reasonable match to the electron diffraction spectrum. It would be interesting to examine whether the fused-planar isomer Au_{21C}^- could fit the electron diffraction since MP2 calculation (Table 1) indicates that Au_{21C}^- is energetically much more favorable than hollow-tubular isomers of Au_{21}^-.

In summary, our unbiased global-minimum search suggests that pyramidal, fused planar, and hollow tubular are three generic structures for the low-lying isomers of Au_{21}^-. Furthermore, MP2 calculation suggests that the lowest-energy isomer likely exhibits fused-planar structure. We also showed that the simulated spectra of the pyramidal isomers alone do not match the measured PES spectra, suggesting that a major structural transition from pyramidal to nonpyramidal form starts at Au_{21}^-.

Au_{22}^-. For Au_{22}^-, the top-eight low-lying isomers obtained from both the unbiased and motif-based constrained searches are shown in Figure 3, together with their corresponding simulated PES spectra. Again, three types of isomer structures can be identified among the low-lying isomers, namely, the pyramidal structure Au_{22A}^-, the planar-fused structures Au_{22B}^-, Au_{22D}^-, and Au_{22G}^-, and the hollow-tubular structures Au_{22C}^-, Au_{22E}^-, Au_{22F}^-, and Au_{22H}^- with notation 3+6+7+5+1, 3+6+6+6+1, and 2+6+6+6+2, respectively, shown in Figure 3. The leading lowest-energy isomer Au_{22A}^- (based on the DFT calculation) gives a very low electron-binding energy. The simulated spectrum of Au_{22A}^- matches the weak feature on the low binding energy side (near 3.3 eV) and feature A of the measured spectrum (Figure 3), suggesting that the pyramidal isomers were weakly populated in the cluster beam. By closely inspecting the simulated spectra of the six isomers Au_{22C}^- to Au_{22H}^-, we conclude that these isomers can be ruled out as the primary isomer since none matches the first intense peak X at 3.54 eV. Only the simulated spectrum of Au_{22B}^- gives good match to the observed intense peaks X, B, and C. Both

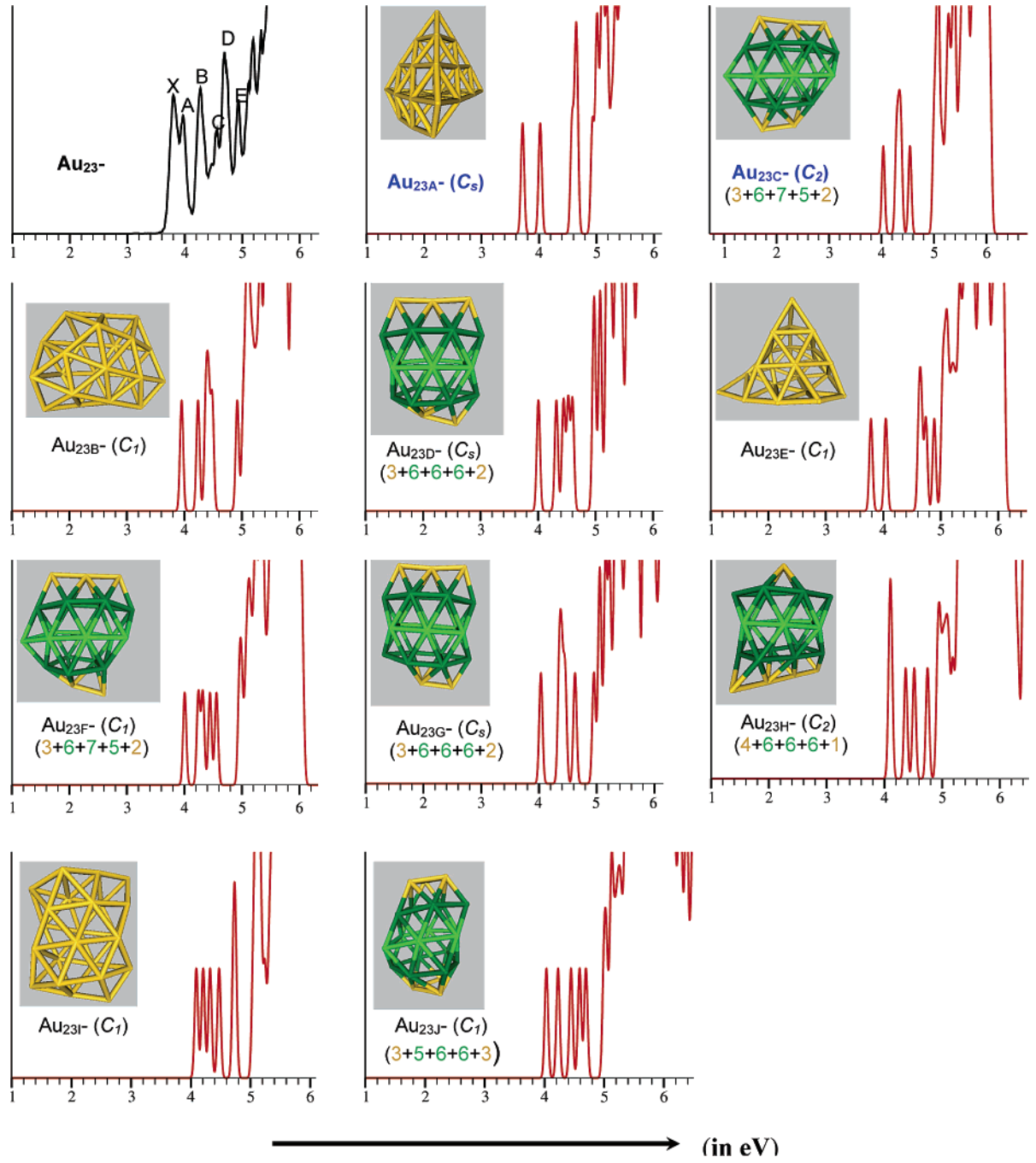

Figure 4. Photoelectron spectrum (black line) measured at 193 nm compared to the simulated PES spectra (red lines) of ten low-lying isomers of cluster Au_{23}^-. The *x*-axis represents binding energy (in eV). The two isomers whose index is highlighted by blue give the best overall fit to the measured spectra.

Au_{22A}^- and Au_{22B}^- may contribute to the feature D. Thus, we conclude that Au_{22B}^- is the *primary* isomer for Au_{22}^- and Au_{22A}^- is a *supplementary* isomer.

Au_{23}^-. For Au_{23}^-, ten low-lying isomers obtained from the searches are shown in Figure 4, together with their corresponding simulated PES spectra. Again, the low-lying population of Au_{23}^- exhibit three types of representative structures, namely, pyramidal, fused planar, and hollow tubular. The latter structure typically contains a tube-like motif such as 6+6+6, 6+7+5, 5+6+6, or 6+7+6, as highlighted in green color in Figure 4. The lowest-lying isomer Au_{23A}^- (based on DFT calculation) is a pyramidal isomer, and Au_{23E}^- is a pyramid-based irregular cage. Among the top 10 low-lying isomers, Au_{23A}^- may be considered as the *primary* isomer since Au_{23A}^- gives reasonable match to the peak X, A, C, D, and E of the measured spectrum. Au_{23E}^- fits the measured spectra reasonably well, but it is about 0.18 eV higher in energy than the lowest-energy isomer Au_{23A}^-. The hollow-tubular isomer Au_{23C}^- may be considered as a *supplementary* isomer since its spectrum matches the locations of peak A, B, and C fairly well. In summary, as in the cases of Au_{21}^- and Au_{22}^-, a low-lying pyramidal isomer Au_{23A}^- alone cannot fully match the measured spectrum. The pyramidal and hollow-tubular isomers together can contribute multiple features near the threshold of the measured PES spectrum.

Au_{24}^-. For Au_{24}^-, nine low-lying isomers obtained from unbiased and motif-based constrained searches are shown in Figure 5, together with their corresponding simulated PES spectra. As shown in Figure 5, the measured spectrum of Au_{24}^- is relatively

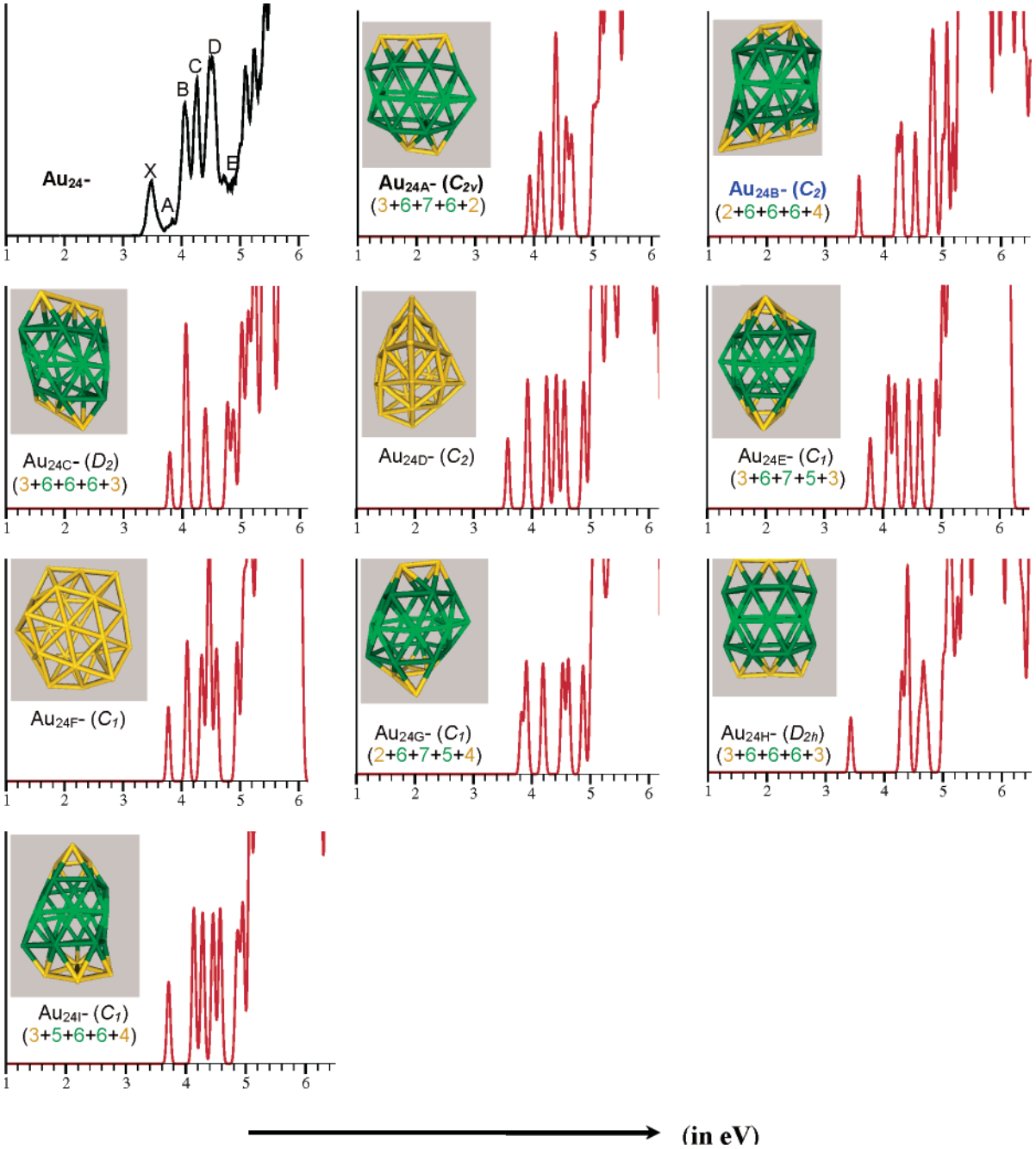

Figure 5. Photoelectron spectrum (black line) measured at 193 nm compared to the simulated PES spectra (red lines) of nine low-lying isomers of cluster Au_{24}^-. The *x*-axis represents binding energy (in eV).

simple with a sizable HOMO−LUMO gap followed by three well-defined and intense peaks B, C, and D. A weak feature A appears at ∼3.85 eV binding energy in the HOMO−LUMO gap region. The characteristically low first VDE and the sizable HOMO−LUMO gap can be used to rule out six low-lying isomers, i.e., Au_{24C} to Au_{24G}^- and Au_{24I}^-. The VDE of Au_{24H}^- is in good agreement with the experiment, but its symmetry seems to be too high, yielding rather simple PES spectra inconsistent with the experiment. We assigned isomer Au_{24B}^- as the *primary* isomer responsible for the experiment. Even though the first VDE of Au_{24B}^- is about 0.09 eV larger than that of the experiment, the energy gap between the first and second intense peak (reflection of relatively larger HOMO−LUMO gap of Au_{24}^- than other clusters in the size range of $n = 21-25$) as well as the higher binding energy features of Au_{24B}^- give the best match to the observed spectrum. Note that Au_{24B}^- is nearly isoenergetic with the lowest-energy isomer Au_{24A}^-. Au_{24A}^- might be considered as a *supplementary* isomer since it contributes to weak feature A. However, the A feature is very weak, suggesting the population of the supplementary isomer was much less than the primary isomer. Note also that the pyramidal structure is not among the top candidates for the lowest-lying cluster of Au_{24}^-. The fact that both Au_{24A}^- and Au_{24B}^- exhibit hollow-tubular structures suggests that a transition from pyramid-based structures (shown in the size range of Au_{18}^- to Au_{23}^-) to hollow-tubular structures is likely to occur at Au_{23}^- and Au_{24}^-. A similar conclusion has also been drawn by Xing et al.[23] However, the isomer (24G in ref 23) which fits the electron diffraction spectra the best is not among the top 10 lowest-energy isomers obtained at the PBE/DNP level of theory. Calculations at MP2 or higher level theory are needed to determine their relative stability.

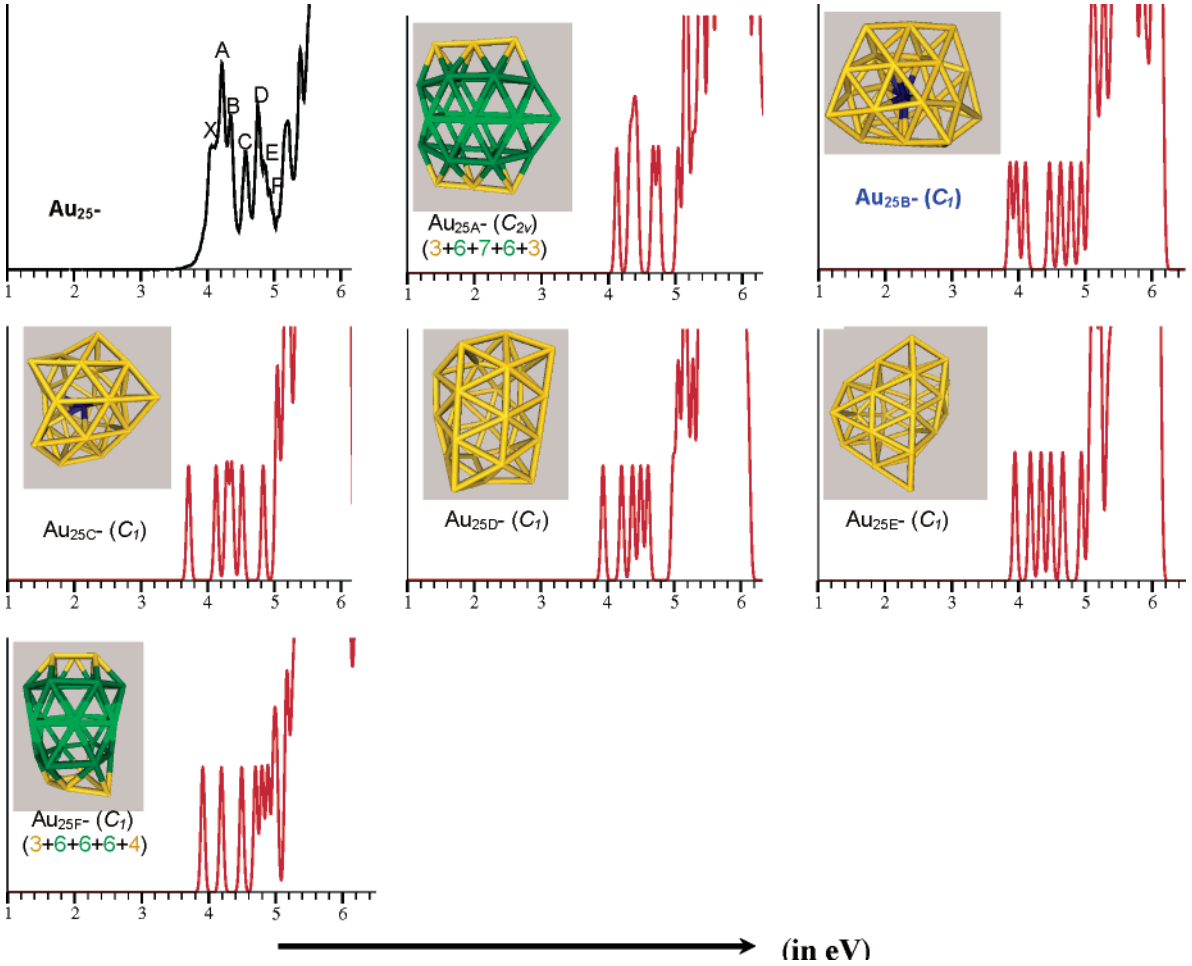

Figure 6. Photoelectron spectrum (black line) measured at 193 nm compared to the simulated PES spectra (red lines) of six low-lying isomers of cluster Au_{25}^- obtained from unbiased search. The *x*-axis represents binding energy (in eV). Atom in dark blue represents inner (endohedral) gold atoms, marking the onset of the structural transition from hollow-tubular to compact structure.

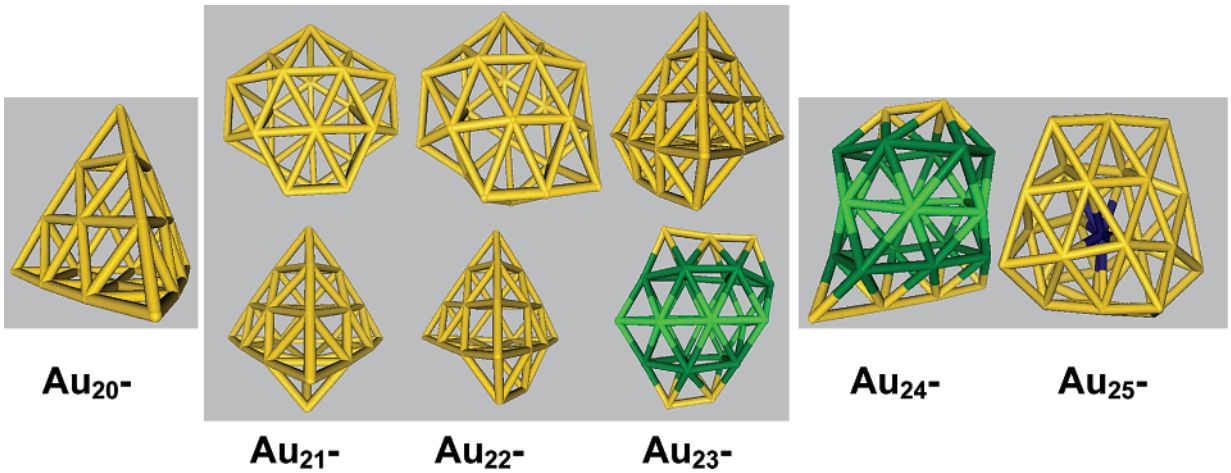

Figure 7. Graphitic illustration of the structural evolution of gold anion clusters from pyramidal Au_{20}^- to fused-planar Au_{21}^- and Au_{22}^- to tubular Au_{23}^- and Au_{24}^- to core/shell compact Au_{25}^-.

Au_{25}^-. We display six low-lying isomers of Au_{25}^- together with their corresponding simulated PES spectra in Figure 6. It is noteworthy that we observed a large population of both irregular cage and core/shell isomers of Au_{25}^- clusters from the global-minimum search. The core/shell compact isomers typically contain an endohedral atom (highlighted by the blue-colored atom for Au_{25B}- and Au_{25C}- in Figure 6), whereas the irregular cages (Au_{25D}- and Au_{25E}-) or hollow-tubular cluster (Au_{25A}- and Au_{25F}-) have larger interior space than the compact isomers.

A distinct feature of the measured spectrum is the presence of three closely spaced peaks X, A, and B in the range of 3.8 to 4.4 eV binding range, followed by four closely spaced peaks C, D, E, and F in the range of 4.4 to 5.0 eV binding energies.

TABLE 2: Electronic Energies (in a.u.) of the Leading Candidates for Lowest-Energy Clusters Calculated at PBEPBE/LANL2DZ Level of Theory, and the Relative Energies ΔE (in eV) with Respect to the Lowest-Energy Cluster for Au_n^- ($n = 22-25$)[a]

cluster	PBEPBE/ LANL2DZ	ΔE
	Au_{22}^-	
A	**−2981.1124224**	**0.000**
B	**−2981.1112637**	**0.032**
C	−2981.1089437	0.095
D	−2981.1058855	0.178
E	−2981.1055790	0.186
F	−2981.1054229	0.190
G	−2981.1038779	0.233
H	−2981.1000896	0.336
	Au_{23}^-	
A	**−3116.6308634**	**0.000**
B	−3116.6298397	0.027
C	**−3116.6297982**	**0.028**
D	−3116.6282644	0.070
E	−3116.6243111	0.178
F	−3116.6237090	0.194
G	−3116.6236418	0.196
H	−3116.6221290	0.237
I	−3116.6197532	0.302
J	−3116.6176917	0.358
	Au_{24}^-	
A	−3252.1279786	0.000
B	**−3252.1277685**	**0.006**
C	−3252.1256993	0.062
D	−3252.1233304	0.126
E	−3252.1227014	0.144
F	−3252.1224170	0.151
G	−3252.1222618	0.156
H	−3252.1222511	0.156
I	−3252.1197672	0.223
	Au_{25}^-	
A	−3387.6478220	0.000
B	**−3387.6466782**	**0.031**
C	−3387.6408839	0.189
D	−3387.6385783	0.252
E	−3387.6362912	0.314
F	−3387.6306318	0.468

[a] Bold-faced values denote the primary and/or supplementary isomers whose simulated PES spectra match the measured spectrum.

TABLE 3: Experimental First Vertical Detachment Energies (VDEs) for Au_n^- ($n = 21-25$) Compared to the Theoretical Values for the Candidate Lowest-Energy Clusters That Give the Best Match to the First Intense Peak of the Measured Spectra[a]

	VDE (theoretical)	VDE(experimental)
Au_{21C}^-	3.912	3.93 ± 0.03
Au_{22B}^-	3.587	3.54 ± 0.03
Au_{23A}^-	3.713	3.80 ± 0.03
Au_{24B}^-	3.574	3.49 ± 0.03
Au_{25B}^-	3.873	4.04 ± 0.03

[a] All energies are in eV.

Among the six isomers, it appears that the simulated spectrum of the core/shell isomer Au_{25B}^- is in best agreement with the experimental data. We therefore assign Au_{25B}^- as the *primary* isomer. The remaining five isomers all show relatively large energy gaps between the first and second intense peaks and may be ruled out. Note that the energy difference between Au_{25B}^- and Au_{25A}^- is merely 0.031 eV at the DFT level (Table 2). Calculations at MP2 or higher level theory are needed to determine their relative stability. However, the good agreement between the experimental and simulated spectra lends support for the isomer Au_{25B}^-, suggesting that a structural transition from hollow-tubular structure at Au_{24}^- to core/shell compact structure occurs at Au_{25}^-.

Conclusions

We have carried out a joint experimental and theoretical investigation to elucidate low-lying structures and structural evolution of Au_n^- clusters within the size range of $n = 21-25$. The global-minimum search revealed complexity of the gold anion clusters in this size range, that is, full of low-lying isomers with a variety of pyramidal, fused-planar, hollow-tubular, and core/shell compact structures. The transition among these structures within the narrow size range of $n = 21-25$ can be conveniently illustrated in Figure 7. To a certain degree, the very stable pyramidal Au_{20} cluster plays an important role in the larger clusters $n = 21-23$. However, dominant isomers for Au_{21}^- and Au_{22}^- are already of fused-planar types (clusters can be viewed as fusion of two planar gold clusters). Hence we conclude that a major structural transition from the pyramidal to nonpyramidal occurs at Au_{24}^-. At Au_{24}^- the low-lying population is dominated by hollow-tubular types. At Au_{25}^-, the global-minimum search indicates that both core/shell and irregular hollow-cage structures are competitive in the population of low-lying isomers, suggesting the onset of the transition from hollow-tubular at Au_{24}^- to core/shell compact structures at Au_{25}^-. It is interesting to point out that starting from the 3D Au_n^- cluster at $n = 13$, only at Au_{25}^- does the cluster begin to possess an inner *endohedral* atom in the low-lying isomer population. It is conceivable that such a core/shell compact structure may become the dominant structural type in larger clusters beyond $n = 25$, as corroborated by the results of the Au_{32}^- cluster.[33]

The comparison of simulated/measured PES spectra provides additional support on the existence of rich structural types and transitions for gold anion clusters in such a small size range. An important question for future study is, in the size range of $n = 26-55$, will the gold anion clusters maintain a single type of generic structure, namely the low-symmetry core/shell compact, or will other generic structures appear? Study in this direction is under way.

Acknowledgment. We thank Dr. J. Li for valuable discussions. The theoretical work done at Nebraska was supported by grants from the DOE's Office of Basic Energy Sciences (DE-FG02-04ER46164), National Science Foundation (CHE-0427746, CHE-0314577, DMI-0210850), the John Simon Guggenheim Foundation, the Nebraska Research Initiative, and the UNL Research Computing Facility. The experimental work done at Washington State was supported by the National Science Foundation (CHE-0349426) and the John Simon Guggenheim Foundation, and it was performed at the EMSL, a national scientific user facility sponsored by the DOE's Office of Biological and Environmental Research and located at the Pacific Northwest National Laboratory, operated for DOE by Battelle.

References and Notes

(1) Haruta, M. *Catal. Today* **1997**, *36*, 153.

(2) Whetten, R. L.; Khoury, J. T.; Alvarez, M. M.; Murthy, S.; Vezmar, I.; Wang, Z. L.; Stephens, P. W.; Cleveland, C. L.; Ludedtke, W. D.; Landman, U. *Adv. Mater.* **1996**, *5*, 8.

(3) Mirkin, C. A.; Letsinger, R. L.; Mucic, R. C.; Storhoff, J. *Nature (London)* **1996**, *382*, 607.

(4) Alivisatos, A. P.; Johnsson, K. P.; Peng, X.; Wilson, T. E.; Loweth, C. J.; Bruchez, M. P.; Schultz, P. G. *Nature (London)* **1996**, *382*, 609.

(5) Pyykkö, P. *Angew. Chem. Int. Ed.* **2004**, *43*, 4412.

(6) Schwerdtfeger, P. *Angew. Chem. Int. Ed.* **2003**, *42*, 1982.

(7) Häkkinen, H.; Moseler, M.; Landman, U. *Phys. Rev. Lett.* **2002**, *89*, 033401.

(8) Furche, F.; Ahlrichs, R.; Weis, P.; Jacob, C.; Gilb, S.; Bierweiler, T.; Kappes, M. M. *J. Chem. Phys.* **2002**, *117*, 6982.

(9) Wang, J.; Wang, G. H.; Zhao, J. *Phys. Rev. B.* **2002**, *66*, 35418.

(10) Häkkinen, H.; Yoon, B.; Landman, U.; Li, X.; Zhai, H. J.; Wang, L. S. *J. Phys. Chem. A.* **2003**, *107*, 6168.

(11) Lee, H. M.; Ge, M.; Sahu, B. R.; Tarakeshwar, P.; Kim, K. S. *J. Phys. Chem. B.* **2003**, *107*, 9994.

(12) Xiao, L.; Wang, L. *Chem. Phys. Lett.* **2004**, *392*, 452.

(13) Grönbeck, H.; Broqvist, P. *Phys. Rev. B.* **2005**, *71*, 073408.

(14) Remacle, F.; Kryachko, E. *S. J. Chem. Phys.* **2005**, *122*, 044304.

(15) Olson, R. M.; Varganov, S.; Gordon, M. S.; Metiu, H.; Chretien, S.; Piecuch, P.; Kowalski, K.; Kucharski, S. A.; Musial, M. *J. Am. Chem. Soc.* **2005**, *127*, 1049.

(16) (a) Han, Y. K. *J. Chem. Phys.* **2006**, *124*, 024316. (b) Diefenbach, M.; Kim, S. *J. Phys. Chem. B.* **2006**, *110*, 21639.

(17) Walker, A. V. *J. Chem. Phys.* **2005**, *122*, 94310.

(18) Fa, W.; Luo, C.; Dong, J. *Phys. Rev. B.* **2005**, *72*, 205428.

(19) Koskinen, P.; Hakkinen, H.; Seifert, G.; Sanna, S.; Frauenheim, Th.; Moseler, M. *New J. Phys.* **2006**, *8*, 9.

(20) Li, J.; Li, X.; Zhai, H. J.; Wang, L. S. *Science* **2003**, *299*, 864.

(21) Bulusu, S.; Li, X.; Wang, L. S.; Zeng, X. C. *Proc. Natl. Acad. Sci. U.S.A.* **2006**, *103*, 8326.

(22) Bulusu, S.; Zeng, X. C. *J. Chem. Phys.* **2006**, *125*, 154303.

(23) Xing, X.; Yoon, B.; Landman, U.; Parks, J. H. *Phys. Rev. B.* **2006**, *74*, 165423.

(24) Häkkinen, H.; Moseler, M.; Kostko, O.; Mrgner, N.; Hoffmann, M. A.; Issendorff, B. v. *Phys. Rev. Lett.* **2004**, *93*, 093401.

(25) Garzon, I. L.; Michaelian, K.; Beltran, M. R.; Posada, A.; Amarillas, P.; Ordejon, E.; Artacho, D.; Sanchez-Portal; Soler, J. M. *Phys. Rev. Lett.* 1**998**, *81*, 1600.

(26) Johansson, M. P.; Sundholm, D.; Vaara, J. *Angew. Chem. Int. Ed.* **2004**, *43*, 2678.

(27) Gu, X.; Ji, M.; Wei, S. H.; Gong, X. G. *Phys. Rev. B.* **2004**, *70*, 205401.

(28) Soule de Bas, B.; Ford, M. J.; Cortie, M. B. *J. Mol. Struct. (THEOCHEM)* **2004**, *686*, 193.

(29) Gao, Y.; Zeng, X. C. *J. Am. Chem. Soc.* **2005**, *127*, 3698.

(30) Wang, J.; Jellinek, J.; Zhao, J.; Chen, Z.; King, R. B.; Schleyer, P. V. R. *J. Phys. Chem A* **2005**, *109*, 9265.

(31) Fernández, E. M.; Soler, J. M.; Balbás, L. C. *Phys. Rev. B.* **2006**, *73*, 235433.

(32) Fa, W.; Dong, J. *J. Chem. Phys.* **2006**, *124*, 114310.

(33) Ji, M.; Gu, X.; Li, X.; Gong, X.; Li, J.; Wang, L. S. *Angew. Chem. Int. Ed.* **2005**, *44*, 7119.

(34) Wang, L. S.; Chen, H. S.; Fan, J. *J. Chem. Phys.* **1995**, *102*, 9480.

(35) Wales, D. J.; Scheraga, H. A. *Science* **1999**, *285*, 1368. Doye, J. P. K.; Wales, D. J. *New J. Chem.* **1998**, 773.

(36) Yoo, S.; Zeng, X. C. *Angew. Chem. Int. Ed.* **2005**, *44*, 1491.

(37) Perdew, J. P.; Burke, K.; Ernzerhof, M. *Phys. Rev. Lett.* **1996**, *77*, 3865.

(38) DMol^3 is a density functional theory program distributed by Accelrys, Inc.; Delley, B. *J. Chem. Phys.* **1990**, *92*, 508.

(39) Frisch, M. J.; Trucks, G. W.; Schlegel, H. B.; Scuseria, G. E.; Robb, M. A.; Cheeseman, J. R.; Montgomery, J. A., Jr.; Vreven, T.; Kudin, K. N.; Burant, J. C.; Millam, J. M.; Iyengar, S. S.; Tomasi, J.; Barone, V.; Mennucci, B.; Cossi, M.; Scalmani, G.; Rega, N.; Petersson, G. A.; Nakatsuji, H.; Hada, M.; Ehara, M.; Toyota, K.; Fukuda, R.; Hasegawa, J.; Ishida, M.; Nakajima, T.; Honda, Y.; Kitao, O.; Nakai, H.; Klene, M.; Li, X.; Knox, J. E.; Hratchian, H. P.; Cross, J. B.; Bakken, V.; Adamo, C.; Jaramillo, J.; Gomperts, R.; Stratmann, R. E.; Yazyev, O.; Austin, A. J.; Cammi, R.; Pomelli, C.; Ochterski, J. W.; Ayala, P. Y.; Morokuma, K.; Voth, G. A.; Salvador, P.; Dannenberg, J. J.; Zakrzewski, V. G.; Dapprich, S.; Daniels, A. D.; Strain, M. C.; Farkas, O.; Malick, D. K.; Rabuck, A. D.; Raghavachari, K.; Foresman, J. B.; Ortiz, J. V.; Cui, Q.; Baboul, A. G.; Clifford, S.; Cioslowski, J.; Stefanov, B. B.; Liu, G.; Liashenko, A.; Piskorz, P.; Komaromi, I.; Martin, R. L.; Fox, D. J.; Keith, T.; Al-Laham, M. A.; Peng, C. Y.; Nanayakkara, A.; Challacombe, M.; Gill, P. M. W.; Johnson, B.; Chen, W.; Wong, M. W.; Gonzalez, C.; Pople, J. A. *Gaussian 03, Revision C.02*; Gaussian, Inc.: Wallingford, CT, 2004.

(40) Becke, A. D. *Phys. Rev. A.* **1988**, *38*, 3098.

(41) Lee, C.; Yang, W.; Parr, R. G. *Phys. Rev. B.* **1988**, *37*, 785.

(42) Perdew, J. P. *Phys. Rev. B.* **1986**, *33*, 8822.

(43) Vosko, S. H.; Wilk, L.; Nusair, M. *Can. J. Phys.* **1980**, *58*, 1200.

(44) Tao, J.; Perdew, J. P.; Staroverov, V. N.; Scuseria, G. E. *Phys. Rev. Lett.* **2003**, *91*, 146401.

(45) Becke, A. D. *J. Chem. Phys.* **1993**, *98*, 1372.